Available online at www.sciencedirect.com
SCIENCE DIRECT
Journal of Sound and Vibration 293 (2006) 496–509
JOURNAL OF SOUND AND VIBRATION
www.elsevier.com/locate/jsvi

Comparison of wheel/rail noise radiation on Japanese railways using the TWINS model and microphone array measurements

T. Kitagawa[a], D.J. Thompson[b,*]

[a]*Railway Technical Research Institute, 2-8-38, Hikari-cho, Kokubunji, Tokyo 185-8540, Japan*
[b]*ISVR, University of Southampton, Highfield, Southampton, SO17 1BJ, UK*

Accepted 26 August 2005
Available online 18 January 2006

Abstract

The railway noise from conventional narrow-gauge lines in Japan mainly consists of rolling noise. A better understanding of rolling noise is required to reduce the noise at the wayside. In the past, in order to quantify wheel/rail noise, theoretical models, such as TWINS, have been developed, and measurements have been carried out with microphone arrays. The TWINS model has been validated in terms of noise and vibration, and used to predict the rail and wheel contributions to the total noise. Results from microphone arrays often give more prominence to the wheel than these predictions. In this paper, the TWINS model is applied to Japanese railways. Through comparisons of predictions with measurements for four types of wheel and one track type, it is shown that the TWINS model gives reliable predictions. Simulations are presented to represent a microphone array. These show that, in the frequency region where waves propagate freely along the rail, the microphone array can significantly underestimate the rail contribution to the noise.

1. Introduction

Railway noise is radiated from various track and vehicle components, such as the rail, the wheel, the engine or traction motors and other components. For the conventional narrow-gauge lines in Japan, the noise generated by railway vehicles mainly consists of rolling noise and noise from the driving devices in the motor vehicles (traction-motor fan noise and gear noise). Rolling noise is known to be induced by a relative vertical vibration of the wheel and rail due to the roughnesses on the wheel and rail surfaces [1]. Traction-motor fan noise is aerodynamic noise generated by the fan that cools the traction motor.

Fig. 1 shows the contributions of the two noise components at a reference point, which is located at 12.5 m away from the centreline of the nearest track [2]. The A-weighted squared sound pressure is shown on a linear scale, although the totals are stated in dB. The contributions were determined using a microphone array at 6.25 m from the track centreline. The traction-motor fan noise was the most dominant source in the past (Train A). However, in new vehicles, the fan noise has been considerably reduced by the introduction of a newly developed traction motor, and the relative contribution of rolling noise to the total noise is therefore

*Corresponding author. Tel.: +44 23 8059 2510; fax: +44 23 8059 3190.
E-mail addresses: toshiki@rtri.or.jp (T. Kitagawa), djt@isvr.soton.ac.uk (D.J. Thompson).

0022-460X/$ - see front matter
doi:10.1016/j.jsv.2005.08.037

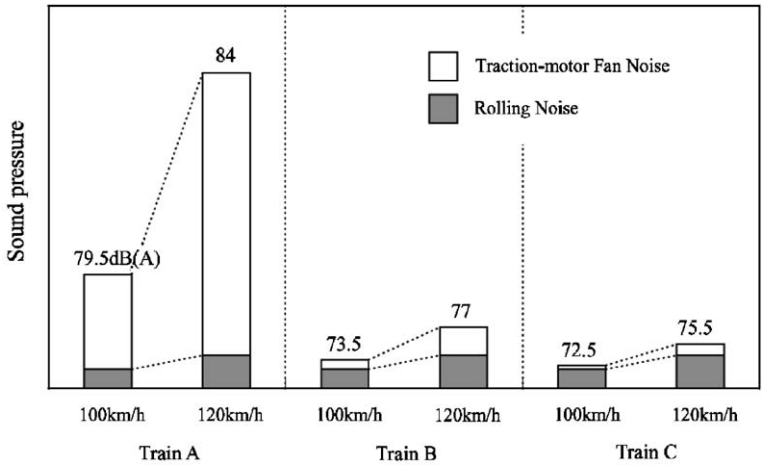

Fig. 1. Noise of the conventional narrow-gauge lines in Japan at 12.5 m from centreline of nearest track [2] (Ground condition: embankment (1.5 m in height), ballast track, plain barrier (2 m in height). Car condition: 10 cars (motor vehicle: 6, trailer: 4), gear ratio: 6. Train A: motors with an outer fan. Train B: motors with an inner fan. Train C: motors with a high-pressure inner fan). Shaded: rolling noise, unshaded: traction-motor fan noise.

larger than before (Train C). Now, in order to reduce the noise at the reference point, a better understanding of rolling noise is required.

In order to quantify wheel/rail noise, theoretical models, such as TWINS, have been developed [1]. The TWINS model has been validated in terms of noise and vibration, and predicted rail and wheel contributions to the total noise using a range of conventional and novel wheel and track designs [3,4]. In other work, measurements have been carried out with microphone arrays to show the spatial distribution of the source positions along a train [2,5–13]. However, the predictions with the TWINS model do not necessarily agree with the measured results obtained with microphone arrays, the latter usually giving less prominence to the rail and more to the wheel.

In order to clarify this point, the paper is composed of two main parts. In the first part, Sections 2–4, a validation of the TWINS model for Japanese railways is carried out. After confirming the applicability of the TWINS model, an attempt is made in Section 5 to investigate the characteristics of wheel/rail noise with reference to the results measured with microphone arrays. In particular, it is investigated whether the assumptions inherent in the use of a microphone array are compatible with an extended source such as the rail.

2. Measurements and preliminary calculations

2.1. Running measurements

A measurement campaign has been carried out and used for the evaluation and validation of the TWINS model for use in the Japanese situation. In this section, the measurement campaign is described briefly. Running measurements were carried out for four different types of wheel, as listed in Table 1. Tests were carried out at various speeds in the range 70–120 km/h. A single track type was used with a 60-type rail on monobloc concrete sleepers and rather hard pads. This is located on a narrow-gauge line, with track gauge 1.067 m. The parameters used here to represent the track are summarised in Table 2. During train pass-bys measurements were made with a microphone at 2 m from the centre of the track and 0.4 m above the railhead. An accelerometer was also located on the rail foot. These measurement locations are shown in Fig. 2. Microphone array measurements were also made at 6.25 m from the track centerline but are not used here.

Table 1
Wheel types tested

Wheel	Radius (mm)	Mass (kg)	Brake	Description
A	405	314	Disc and tread braked (resin block)	Singly curved web
C	430	314	Tread braked (cast iron block)	Straight web
AW	430	292	Disc and tread braked (resin block)	Doubly curved web
CW	430	292	Disc and tread braked (resin block)	Doubly curved web

Table 2
Values of TWINS parameters for the track

	Vertical	Lateral
Rail bending stiffness (Nm^2)	5.32×10^6	1.05×10^6
Rail shear coefficient	0.4	0.4
Rail loss factor	0.01	0.01
Mass per length (kg/m)	60	
Cross receptance level (dB)	−12	
Pad stiffness (N/m)	7.0×10^8	8.5×10^7
Pad loss factor	0.25	0.25
Sleeper mass (1/2 sleeper) (kg)	80	
Distance between sleepers (m)	0.625 (0.6–0.65)	
Ballast stiffness (N/m)	6.7×10^7	3.4×10^7
Ballast loss factor	2.0	2.0

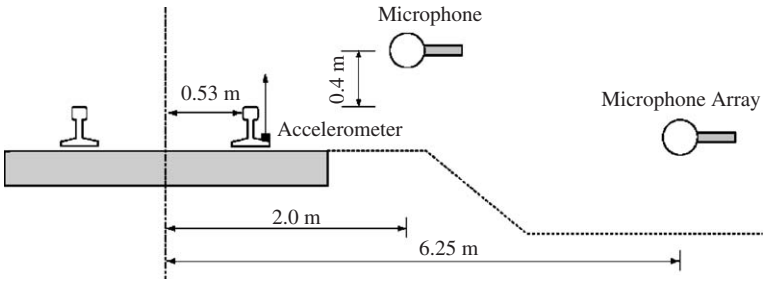

Fig. 2. Diagram of measurement positions.

2.2. Tuning of the track parameters

Static tests have been performed in order to determine appropriate calculation parameters for the track [14]. Measurements are limited to frequencies up to 1.2 kHz. Fig. 3(a) shows the predicted and measured accelerances in the vertical direction. A comparison of the measured results with the predictions of two models available in TWINS (rodel: continuously supported beam model, tinf: periodically supported beam model) shows good agreement.

As the rail is supported periodically, the tinf model predicts the pinned–pinned resonances and a difference in frequency response between the two measured positions (above a sleeper and at mid-span). However, the phenomena associated with the pinned–pinned resonance cannot be seen clearly in the measurements. Fig. 3(b) shows the decay rates of rail vibration in the vertical direction. A satisfactory agreement is obtained between the predicted and measured decay rates, confirming the choice of pad stiffness in the model.

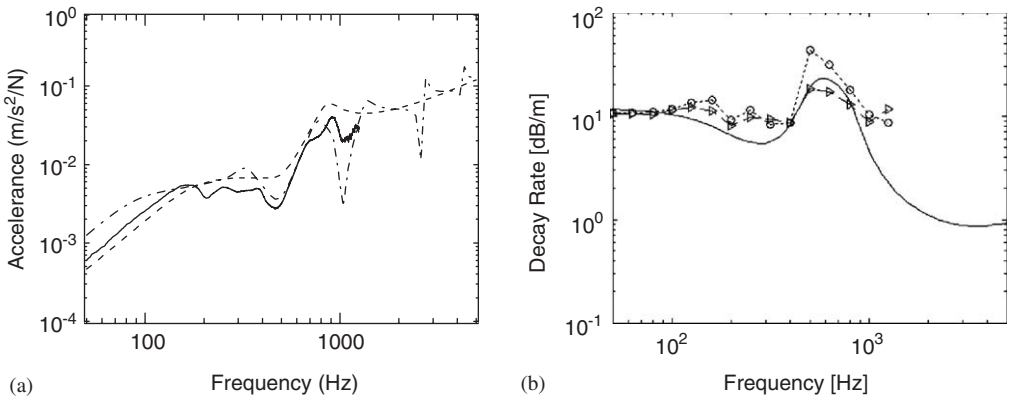

Fig. 3. (a) Vertical point accelerance above sleeper, —, measured result; – – –, rodel model, – · –, tinf model. (b) Decay rate of vertical rail vibration with distance. ○ and △, measured; —, rodel model.

Table 3
Natural frequencies for CW wheel

n	Zero-nodal-circle		Radial		One-nodal-circle	
	Pred.	Meas.	Pred.	Meas.	Pred.	Meas.
0	313	336	2270	2470	1630	1730
1	163	—	744	—	1910	—
2	418	441	1070	1260	2480	—
3	1090	1120	1680	1910	2850	—
4	1920	1980	2350	—	3920	—

n, number of nodal diameters; Pred., predicted natural frequency; Meas., measured natural frequency (Hz) (from Ref. [15]).

2.3. Tuning of the wheel parameters

For the four types of wheel listed in Table 1, the modal bases have been predicted using the finite element software and the modal superposition method. Principal wheel modes of vibration are categorised by the number of nodal diameters (n) and the number of nodal circles (m). Predicted natural frequencies for the CW wheel are listed in Table 3. Also listed are measured natural frequencies [15], from which it can be seen that reasonable agreement has been achieved, although differences of up to 10% are found for the radial modes. To improve these further would require details of the geometry of the actual wheel rather than the nominal design. However, these differences do not have a significant effect on the radiated sound particularly when one-third octave bands are used.

For the modal damping ratio, no measured data were available from the measurement campaign. Therefore, typical values are used of 10^{-4} for modes with two or more nodal diameters, and higher values for modes with one or no nodal diameters [16].

2.4. Roughness inputs

In order to evaluate noise and vibration with the TWINS model, a roughness spectrum is required for input to the calculations. As no data were available corresponding to the tests, the TWINS calculations have been carried out by using ‘standard’ roughness spectra from European railway wheels and rails [17]. A tread-braked spectrum is used for wheel C and a disc-braked spectrum for the other wheels.

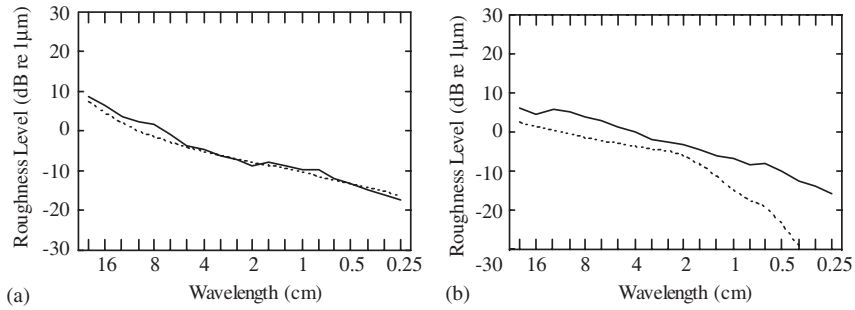

Fig. 4. (a) Rail roughness spectra, — 'standard' based on average of six European sites, ····· measurement on one Japanese site, (b) wheel roughness spectra, — 'standard' based on average of 37 European disc-braked wheels, ····· measurement on one Japanese wheel.

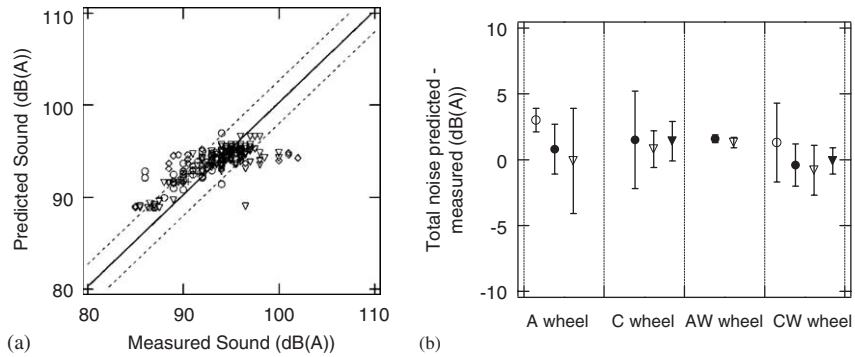

Fig. 5. (a) Predicted noise plotted against measured noise for all cases. ◇, A-type wheel; ○, C-type wheel; +, AW-type wheel; ▽, CW-type wheel. (b) Total predicted noise minus measured noise in dB(A) with error bars indicating range of ± one standard deviation. ○, 70 km/h; ●, 100 km/h; ▽, 110 km/h; ▼, 120 km/h.

The standard roughness spectra are shown in Fig. 4 for the rail and a disc-braked wheel. Although little data is available of roughness from Japan, two roughness spectra obtained from Japan are shown. The standard rail roughness can be seen to be comparable to that from Japan. For the wheel, the standard roughness spectra are different from those obtained for Japanese wheels. However, the roughness measurement for the Japanese wheel is obtained from only one wheel. The standard spectra are obtained by averaging the results of 30 or more wheels, and are therefore considered to be more reliable for use in the TWINS calculations.

3. Results for the validation

In this section, the results of the predicted noise are compared with the measurements. Other results are given in Ref. [18]. In the predictions, the mono-bloc sleeper model is used in order to introduce modal sleeper behaviour and frequency dependent ballast properties. This section presents calculations of noise carried out using the continuously supported track model (rodel) and calculated track decay rates.

3.1. Comparison of overall sound levels

Fig. 5(a) shows the predicted noise plotted against the measured noise in terms of A-weighted levels. The individual points represent different runs for one of the four wheel/track combinations. The solid line corresponds to the mean difference between predictions and measurements, and the dashed lines show a range of ± one standard deviation. It is clear that the overall trends are well predicted. Fig. 5(b) shows the total noise predicted minus measured noise in dB(A) for each wheel/track combination, with error bars representing

the range of ± one standard deviation in each case. It can be seen that for most of the results for the 12 wheel/track/speed combinations the mean is in the range ±1.5 dB. The overall predictions show good agreement with the measured results, although the measured results contain much greater spread. This tends to suggest that the measured noise increases at a lower rate than the predicted noise in Fig. 5(a), but this is exaggerated by the results for the A-wheel at 110 km/h which include measurements between 96 and 102 dB(A). It is also possible that the shape of the assumed roughness spectra may affect the speed dependence of the predicted results.

3.2. Comparison of spectral results

In order to consider the spectral variation, the difference between predicted and measured noise spectra is constructed for each of seven wheel/track/speed combinations for which this data is available (spectra are not available for all the cases given in Fig. 5). Fig. 6 shows the spectral differences as the mean and a range of ± one standard deviation for all cases. Below 250 Hz, the agreement is poor, since the measured results were contaminated by wind noise (the microphone is very close to the track). It can be seen that the results are close to zero; the average difference is −0.8 dB in the whole frequency range from 250 to 8000 Hz. It can be seen that, at high frequencies above 2500 Hz, the results are slightly over-predicted whereas below 1000 Hz the results show a slight under-prediction. These differences are not significant considering that assumed roughness spectra have been used which may differ from the actual ones.

Fig. 7 shows the separate contributions of noise from rail, wheel and sleeper to the total prediction in the form of spectra for two examples. The measured spectra are also shown for comparison. It can be seen that the sleeper is the important source below around 400 Hz, whilst the wheel is the predominant source above 2000 Hz. In the middle frequencies, the dominant component in the total noise depends on the wheel type. For the A-type wheel, the rail becomes dominant in the middle frequencies. On the other hand, for the CW-type wheels, the wheel has almost the same contribution to the total noise as the rail has between 1000 and 2000 Hz. It can be seen from Table 3 that the radial modes of this wheel commence from 1 kHz due to the thin web; the same is true for the AW-type wheel. As discussed above, the differences with measured noise are due to wind noise at low frequencies and possibly due to the assumed roughness spectra in the mid-frequencies.

Fig. 8 shows the spectral differences in rail vibration as the mean and a range of ± one standard deviation for all cases. Some differences exist between measurements and predictions, which may be due to the reliance

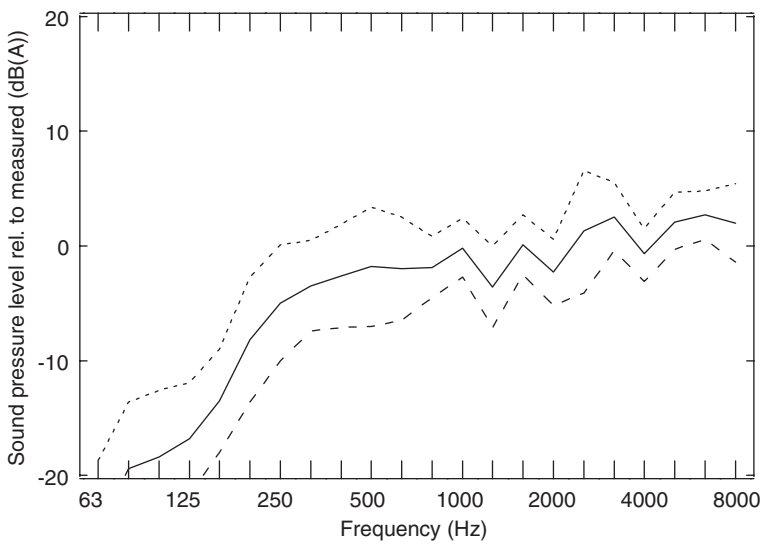

Fig. 6. Average differences between predicted and measured noise spectra for all cases. —, mean; – – –, mean−std deviation; ·····, mean + std deviation.

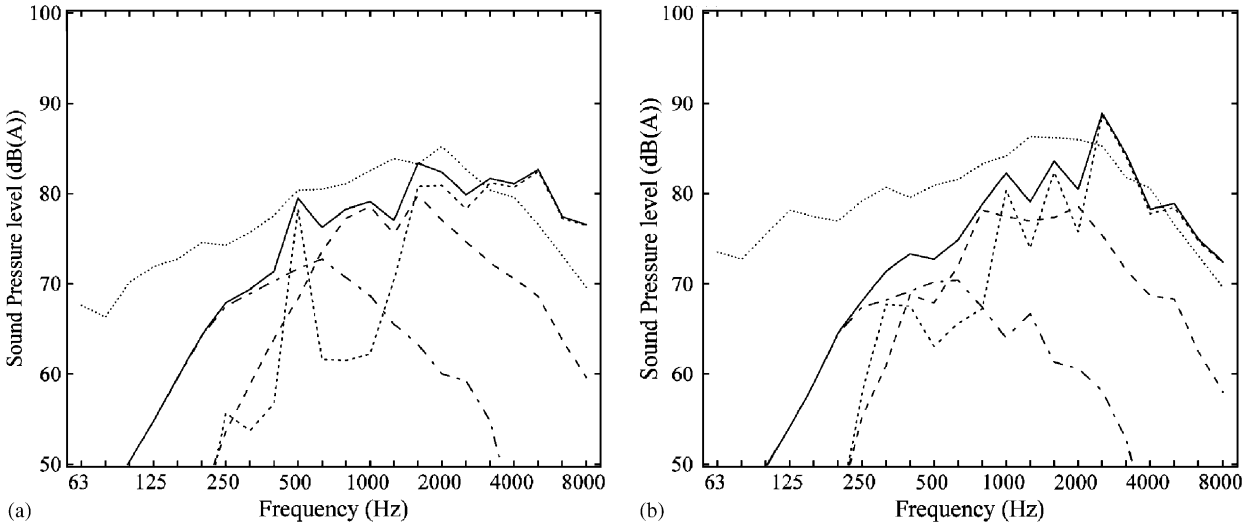

Fig. 7. Predicted noise and measured noise for each wheel ($V = 110$ km/h). ⋯⋯, measured noise; —, predicted noise; − − −, rail; - - -, wheel; − · −, sleeper. (a) A-type wheel. (b) CW-type wheel.

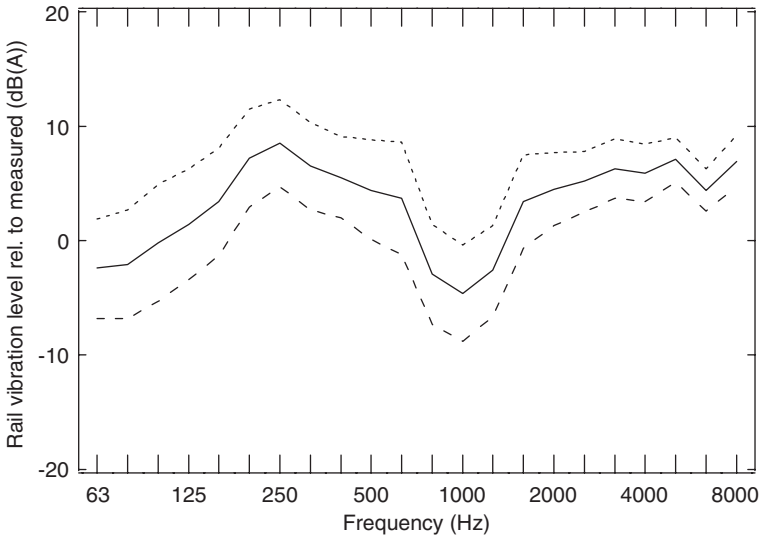

Fig. 8. Average differences between predicted and measured spectra in terms of rail vibration for all cases. —, mean; − − −, mean−std deviation; ⋯⋯, mean + std deviation.

on a single measurement position. Nevertheless, it is clear that the large difference at low frequency found in the noise results is not present here. This confirms that the measured noise includes other components below 250 Hz which are not generated from the wheels and track, i.e. wind noise.

4. Dependence on wheel load

In this section, an attempt to estimate the effect of wheel load on noise will be made by comparing predictions from the TWINS model with measurements. No previous experimental results are available of this effect, although it has been considered theoretically for a particular application in Ref. [19]. Measurements

Table 4
Wheel load condition

Freight vehicle	Vehicle length (m)	Condition 1 (kN)	Condition 2 (kN)
I	20	23.5	64
II	16	21.5	81.5

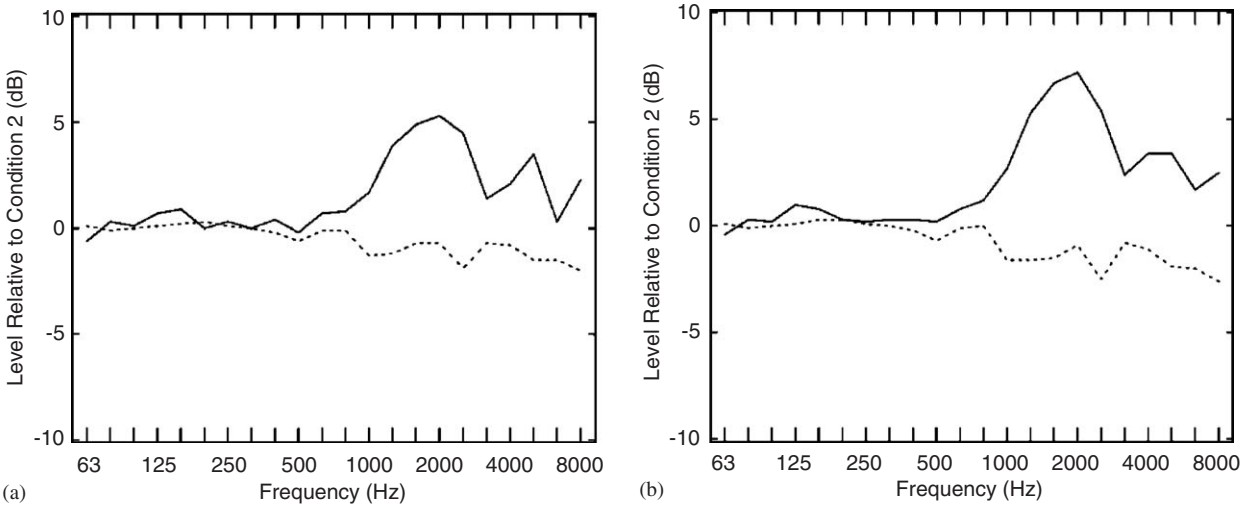

Fig. 9. Predicted difference in contact filter and normal load effects, 100 km/h. —, contact filter; ⋯⋯, contact stiffness. (a) Freight vehicle I and (b) freight vehicle II.

were carried out for two types of freight car, both with A-type wheels (see Table 1) in loaded and unloaded conditions. The wheel load conditions are listed in Table 4.

The TWINS calculations of noise are carried out using the same track and wheel models as above and the same assumed roughness spectrum. In order to estimate the effect of the wheel load, two aspects should be considered: the effect on the contact stiffness and the change in contact filter. The wheel load determines the size of the contact zone between the wheel and rail. Roughness with wavelengths that are small in comparison with the contact patch length is attenuated, and does not excite the wheel/track system as well as long wavelength roughness. The contact patch length determines the wavelength at which the contact filter rolls off. Therefore, it is necessary that the contact filter effect corresponding to the wheel load should be determined.

Fig. 9 shows the predicted difference in contact filter and normal load effects between the two wheel load conditions. Below 800 Hz, the normal load has no significant influence on the noise components. Above 1000 Hz, it is clear that the contact filter effect has greater influence than the contact stiffness. As the wheel load is increased, the whole contact filter curve is shifted to the left. The effective frequency at which the contact filter rolls off reduces as the wheel load is increased. Therefore, the wheel/rail system is significantly influenced due to the contact filtering effect above 1000 Hz, and the increase of the wheel load could lead to some noise reduction.

Fig. 10 shows the overall A-weighted noise level plotted against train speed. It can be seen that in both predictions and measurements the noise reduces as the wheel load increases. The difference between the two wheel load conditions appears to be constant, and independent of train speed. Compared with the measurements, the global trends are predicted well. However, the predictions are all somewhat too high, which may be because the standard roughness spectrum used here again differs from the actual case.

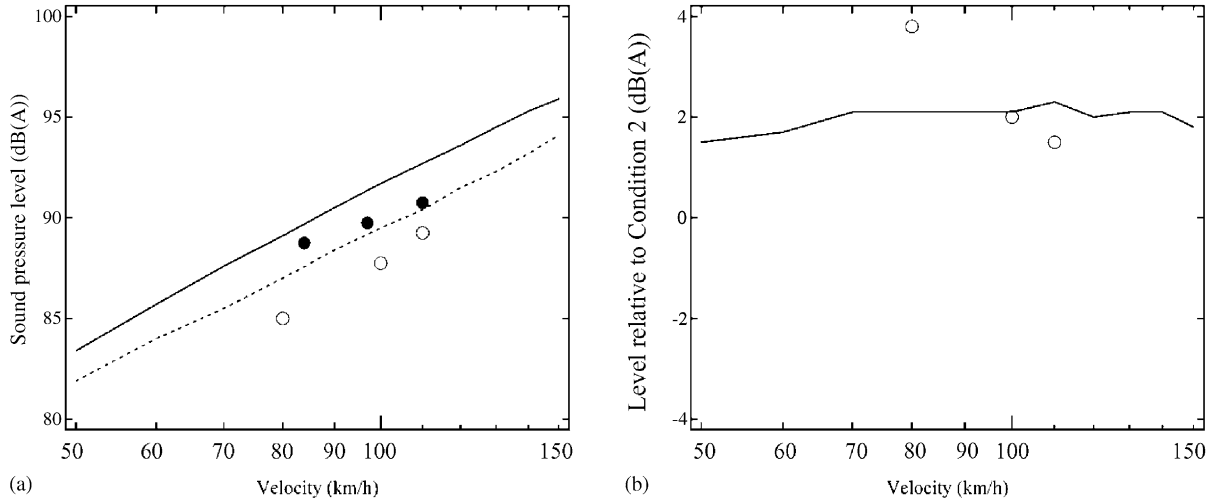

Fig. 10. (a) Overall levels plotted against train speed for freight vehicle I. — , predicted, 23.5 kN; ⋯⋯, predicted, 64 kN; ●, measured, 23.5 kN; ○, measured, 64 kN. (b) Difference in dB(A) between two wheel load conditions. —, predicted; ○, measured results.

5. Microphone array measurements

5.1. Background

Microphone arrays have been widely used in order to identify sound sources on moving trains. For aerodynamic sources this is the main means available to locate sources. However, the technology has also been widely used to study rolling noise [2,5–13]. A common feature of these studies is that they tend to show that the wheel is the dominant source of rolling noise, whereas it is found from theoretical analyses based on models such as TWINS that the rail can be the dominant source in much of the frequency range [3,4]. In this section the nature of the sound radiation from the rail is investigated to determine whether there is a fundamental problem in measuring it using a microphone array.

The microphone array works by deploying a large number of microphones at a particular distance from the track. These may be arranged in a single line, which may be horizontal, to locate sources along the train, or vertical, to locate their height. It may also consist of two perpendicular lines (T or X shapes), fuller 'star' shapes or a full two-dimensional arrangement such as a spiral array [12,13]. The microphone spacing, along with the acoustic wavelength, determines the spatial resolution that is possible. Thus to cover a wide frequency range several spacings may be used. Various forms of processing are used, either in real time or from recorded data.

The basic assumption behind the use of a beam-forming microphone array is usually that the sources to be identified consist of a distribution of *uncorrelated* point sources located in a plane at some known distance from the array. The outputs from each microphone are added together, allowing for some delay and a weighting function, to give the sound arriving from a particular direction.

A rail vibrates as a structural waveguide, transmitting bending waves along its length. These waves generally have a wavelength that is longer than the acoustic wavelength and a relatively low rate of decay with distance. The sound radiated by a rail, which is considered to be an array of *correlated* point sources, has been studied in Ref. [20]. It is shown that, for frequencies above about 250 Hz, the radiation efficiency of a rail can be obtained by solving a two-dimensional problem due to the long wavelength and low decay rate of the vibration. However, most of the sound radiation occurs at an angle to the rail that depends on the ratio of the structural and acoustic wavelengths. Therefore, it is necessary to identify the extent to which the microphone array could 'see' the main rail radiation lobe. To the authors' knowledge, beam-forming microphone arrays have not been used to study the sound radiation from extended line sources.

5.2. Simulation

A modelling approach similar to that used in Ref. [20] has been used here to determine the radiation from a rail. The rail vibration is determined first using the rodel model, as in Section 3. This represents the rail as a Timoshenko beam on layers of springs, masses and springs to represent the rail pads, sleepers and ballast, respectively. Using this model, the vibration is determined at many points along the rail due to a force at $x = 0$. An array of acoustic point sources (in the present study monopoles are used) are defined along the rail and assigned source strengths according to the amplitude and phase of the rail vibration, as indicated in Fig. 11. The number of sources used is chosen according to criteria given in Ref. [20]. The sound pressure generated by each of these sources is calculated at a series of receiver locations at a distance of 5.72 m from the rail and summed to give the total pressure at these locations. The array of receiver locations is moved past the source. This can be seen to represent the sound pressure at a microphone as the rail vibration (due to a single wheel) passes the microphone, apart from the Doppler effect which is ignored here.

In addition, the output from a microphone array is simulated for an equivalent set of positions. The microphone array represents an MY13 array as used by RTRI. This is a one-dimensional array composed of 119 microphones, used horizontally. For each one-third octave band, a different set of up to 17 microphones is selected to give an optimal resolution for this band. This process is simulated in the calculations. The array can be used with different time delays to determine the radiation in different directions, but in the present application, measuring rolling noise, it is used with no time delays in order to extract the sound radiated from the sources directly in front of the array. Even in cases where a swept focus has been used in measuring rolling noise [5] the range of angles considered is only a few degrees.

Fig. 12 shows the distribution of rail vibration amplitude along the rail, the output from a single microphone and the output from a microphone array for two different frequencies. The rail vibration is calculated using the parameters given in Table 2. Also shown are the results that are obtained if the same source distribution is used but the sources are assumed to be incoherent (but with the same total output power).

The results for 125 Hz show that the rail vibration is localised to a region within about 1 m from the forcing point, due to the decay rate of about 10 dB/m. This effectively forms a point source. The results at the single microphone decay gradually with distance whereas the result of the microphone array (here five microphones at a spacing of 1.36 m) gives better localisation of the source.

The results for 1600 Hz, however, show an extended source on the rail, here with a decay rate of 1.6 dB/m. The structural wavelength, Fig. 12(e), is 0.96 m at this frequency, whereas the acoustic wavelength is 0.21 m. Close to the excitation point the presence of a near-field wave can also be seen in Fig. 12(f). The microphone array here has 17 microphones with a spacing of 0.17 m. The distributed nature of the source is reflected in the microphone array results when the sources are incoherent but not for the case when the sources have the correct phase according to the rail vibration. In the latter case, the microphone array only detects the radiation from the region close to the forcing point. The extended line source, however, radiates at an angle to the

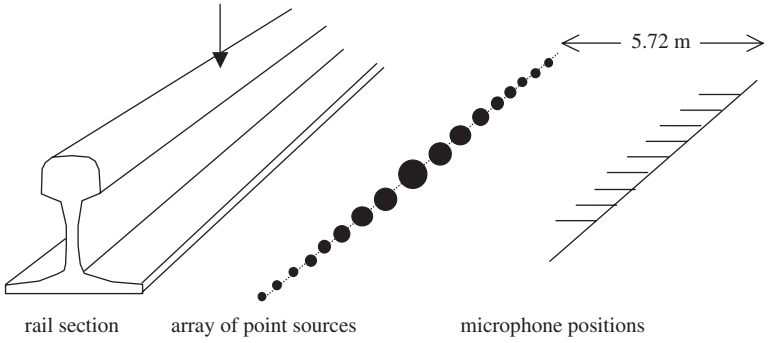

Fig. 11. Modelling method. Vibration on the rail is assigned to the source strengths of an array of point sources. The sound pressure is calculated at the microphone positions.

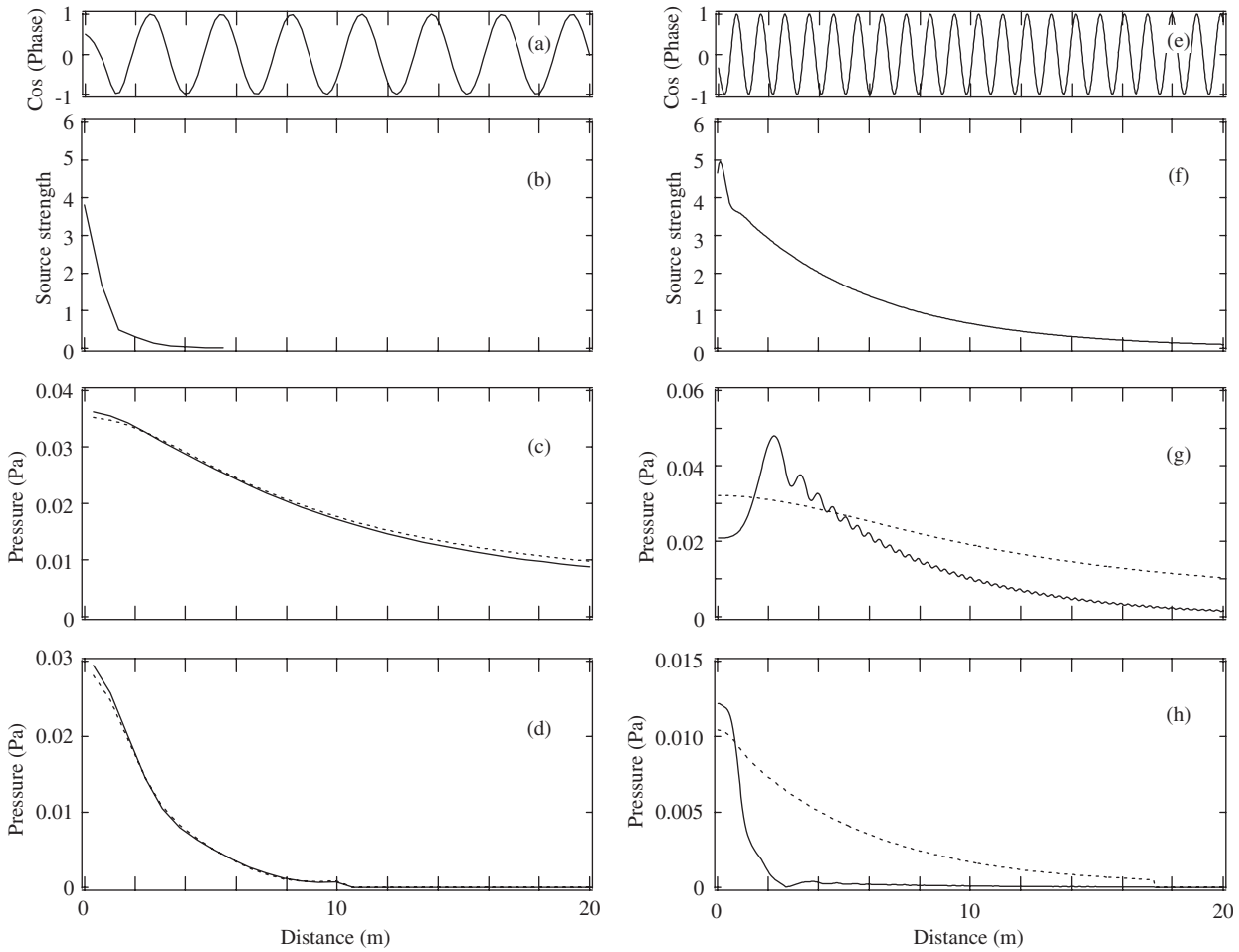

Fig. 12. Simulation results for vertical rail vibration, rail damping loss factor 0.02, other parameters as in Table 2, 125 Hz (left) and 1600 Hz (right). (a,d) Relative phase obtained from rail vibration, (b,f) Relative source strength obtained from rail vibration (arbitrary scale), (c,g) magnitude of sound pressure at single microphone versus distance along the track from the forcing position, (d,h) output from microphone array; —, sources accounting for phase, - - -, incoherent sources.

normal [18], determined from the ratio of the structural and acoustic wavelengths as 13°. At a distance of 5.72 m from the line source this means that the maximum pressure is expected to occur at 2.0 m from the forcing point, which corresponds with the main peak seen in Fig. 12(g).

5.3. Overall result

To quantify the effect of measuring with a microphone array, the squared pressure obtained using the microphone array is integrated along a sufficient length. The equivalent result is also obtained for the set of incoherent sources with the same overall power. The level difference between these two results is used as a measure of the extent to which the microphone array can measure the noise from the rail. This is shown in Fig. 13(a). Note that the results with a level difference below –10 dB are affected by truncation of the integration. For the track studied above, with a pad stiffness of 700 MN/m, free propagation of vertical waves in the rail only occurs above about 1 kHz, whereas with a reduced pad stiffness of 200 MN/m free wave propagation occurs above about 500 Hz. The corresponding track decay rates are shown in Fig. 13(b). The similarity between the track decay rate and the overall effect of the microphone array measurement on the noise obtained from rail vibration can be seen clearly. The microphone array underestimates the rail source in the region where wave propagation occurs. Differences of up to 10 dB are found here. In the region around 800 Hz

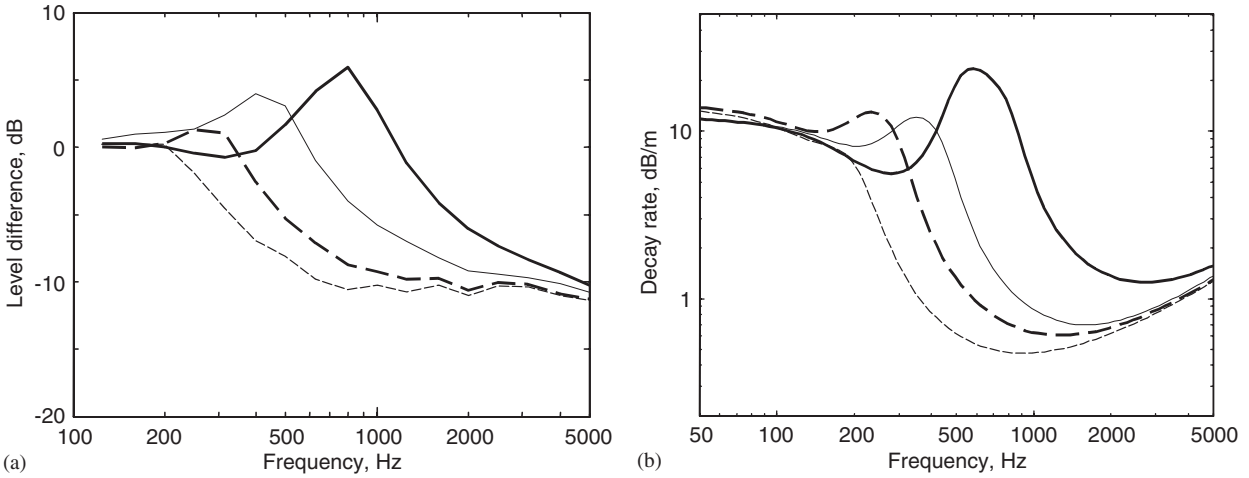

Fig. 13. (a) Overall effect of using microphone array to measure noise from rail vibration. (b) Track decay rates. ——, vertical vibration, rail pad stiffness 700 MN/m; — —, lateral vibration, rail pad stiffness 85 MN/m; —, vertical vibration, rail pad stiffness 200 MN/m; – – –, lateral vibration, rail pad stiffness 40 MN/m.

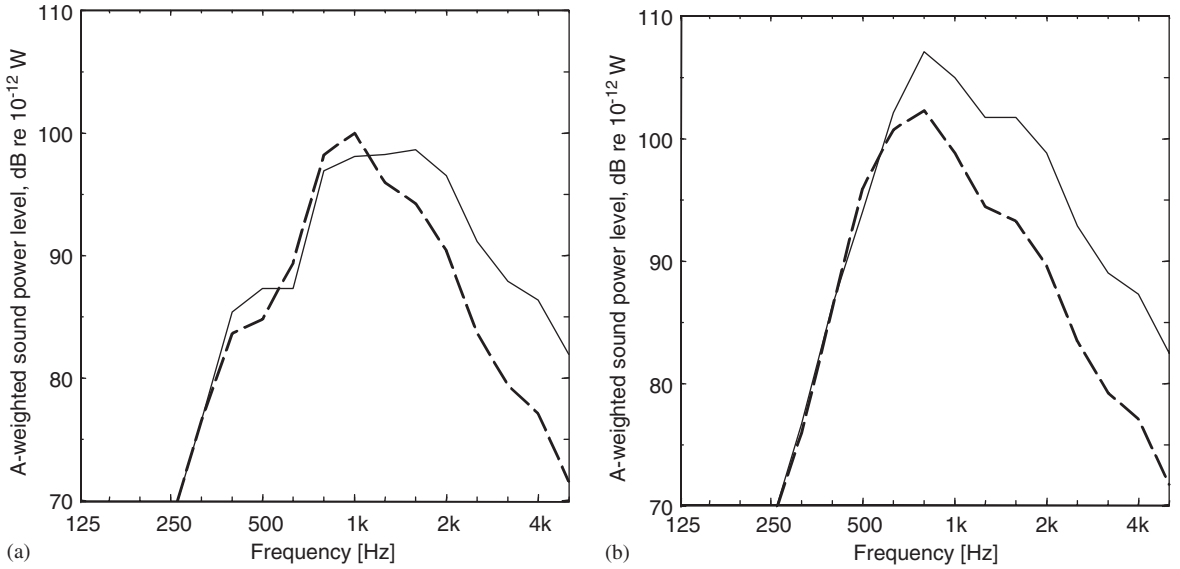

Fig. 14. Effect on rail component of noise using a microphone array. —, actual rail noise; – – –, rail noise inferred from microphone array. (a) Track with 700 MN/m pads. (b) Track with 200 MN/m pads.

(400 Hz for the softer pad) the microphone array *over*-estimates the rail noise. However, this corresponds to a region of very high decay rate associated with the sleeper vibrating as a vibration absorber where the rail contribution is small. Results are also shown for lateral rail vibration; here the wave propagation commences at a lower frequency, but otherwise a similar trend is found. The relation between the decay rate and microphone array error will depend also on the distance of the source from the array and the array length but otherwise there seems to be a direct agreement.

Finally, Fig. 14 gives an estimate of the rail component of noise and that which would be inferred from a microphone array measurement. To obtain this, the predicted vertical and lateral components have been separately modified by the corrections in Fig. 13(a). Clearly, at frequencies above 1 kHz the microphone array tends to underestimate the rail contribution considerably. For the softer rail pad considered above, large

differences are present from 630 Hz upwards. It should be recalled that the wheel component will also be present in the total noise from 1–2 kHz upwards, whereas these estimates are only of the effect on the rail noise. Consequently, the effect may be masked in practice by the presence of the wheel.

6. Summary

In order to validate the TWINS software for rolling noise prediction, a comparison with measurements has been carried out for four wheel/rail combinations of Japanese railways. The TWINS model gives reliable overall noise predictions, provided that the mono-bloc sleeper model is introduced in the TWINS model. It is found that the mean difference in noise between the predictions and measurements is in the range of ± 1.5 dB. In terms of noise spectra, the predictions show a slight under-prediction below 1000 Hz and an over-prediction above 1000 Hz. These differences are in part attributable to the fact that the roughness spectra had to be assumed.

An attempt to estimate the effect of wheel load on rolling noise has been made by using the TWINS model. The TWINS model shows similar trends to the measurements, with a slight reduction in rolling noise as load increases.

Analysis of the performance of a microphone array indicates that a horizontal array (or two-dimensional array) will not detect a large part of the noise from the rail at high frequencies where free wave propagation occurs in the rail. Differences of up to 10 dB are found. This may explain why measurements using microphone arrays tend to emphasise the wheel as the dominant source, whereas using the TWINS model the rail is also found to be an important source in many situations. This could be overcome by adjusting the delays in the microphone array processing to direct it at other angles as well as normal to the track; the processing would also require modification to allow for the coherent nature of the source.

Acknowledgements

The work described here was carried out while the first author was visiting ISVR, University of Southampton, UK.

References

[1] D.J. Thompson, B. Hemsworth, N. Vincent, Experimental validation of the TWINS prediction program for rolling noise, part 1: description of the model and method, *Journal of Sound and Vibration* 193 (1996) 123–135.
[2] T. Kitagawa, Y. Zenda, Y. Abe, Y. Ogata, Sound radiated by vibration of railway wheels, in: *Proceedings of Inter Noise 2001*, The Hague, Netherlands, 2001.
[3] D.J. Thompson, P. Fodiman, H. Mahé, Experimental validation of the TWINS prediction program for rolling noise, part 2: results, *Journal of Sound and Vibration* 193 (1996) 137–147.
[4] C.J.C. Jones, D.J. Thompson, Extended validation of a theoretical model for railway rolling noise using novel wheel and track designs, *Journal of Sound and Vibration* 267 (2003) 509–522.
[5] B. Barsikow, W.F. King III., E. Pfizenmaier, Wheel/rail noise generated by a high-speed train investigated by a line array of microphones, *Journal of Sound and Vibration* 118 (1987) 99–122.
[6] B. Barsikow, Experiences with various configurations of microphone arrays used to locate sound sources on railway trains operated by the DB AG, *Journal of Sound and Vibration* 193 (1996) 283–293.
[7] G. Hölzl, Low noise goods wagons, *Journal of Sound and Vibration* 193 (1996) 359–366.
[8] J.D. van der Toorn, H. Hendricks, T.C. van den Dool, Measuring TGV source strength with Syntacan, *Journal of Sound and Vibration* 193 (1996) 113–121.
[9] M.G. Dittrich, M.H.A. Janssens, Improved measurement methods for railway rolling noise, *Journal of Sound and Vibration* 231 (2000) 595–609.
[10] S. Brühl, A. Röder, Acoustic noise source modelling based on microphone array measurements, *Journal of Sound and Vibration* 231 (2000) 611–617.
[11] C. Hanson, B. Barsikow, Noise sources on Amtrak's high speed train, in: *Proceedings of Inter Noise 2000*, Nice, France, 2000.
[12] A. Nordborg, A. Martens, J. Wedemann, L. Willenbrink, Wheel/rail noise separation with microphone array, in: *Proceedings of Inter Noise 2001*, The Hague, Netherlands, 2001.
[13] K.G. Degen, A. Nordborg, A. Martens, J. Wedemann, L. Willenbrink, M. Bianchi, Spiral array measurements of high-speed train noise, In: *Proceedings of Inter Noise 2001*, The Hague, Netherlands, 2001.

[14] K. Manabe, M. Takigawa, Modal behaviour of a track, RTRI Report, 2001 (in Japanese).
[15] S. Tanaka, H. Minami, K. Akutsu, Y. Zenda, Vibratory characterization of NA-type wheel, *RTRI Report*, 2002 (in Japanese).
[16] C.J.C. Jones, D.J. Thompson, Rolling noise generated by railway wheels with viscoelastic layers, *Journal of Sound and Vibration* 231 (2000) 779–790.
[17] D.J. Thompson, Definition of the reference roughness, ISVR Internal Report for Silent Freight and Silent Track projects, 1997.
[18] T. Kitagawa, D.J. Thompson, Application and validation of the TWINS model for Japanese Railways, ISVR Technical Memorandum, No. 919, University of Southampton, 2003.
[19] D.J. Thompson, C.J.C. Jones, A study of the use of vehicles with small wheels for determining the component of noise from the track, in: *Proceedings of IOA Spring Conference*, Salford, CD-ROM, March 2002.
[20] D.J. Thompson, C.J.C. Jones, N. Turner, Investigation into the validity of two-dimensional models for sound radiation from waves in rails, *Journal of the Acoustical Society of America* 113 (2003) 1965–1974.